Tetrahedron 68 (2012) 5590–5598

Contents lists available at SciVerse ScienceDirect

Tetrahedron

journal homepage: www.elsevier.com/locate/tet

Functionalized organic dyes containing a phenanthroimidazole donor for dye-sensitized solar cell applications

Woochul Lee [a], Youna Yang [a], Nara Cho [b], Jaejung Ko [b,*], Jong-In Hong [a,*]

[a] Department of Chemistry, Seoul National University, Seoul 151-747, Republic of Korea
[b] Department of New Material Chemistry, Korea University, Jochiwon, Chungnam 339-700, Republic of Korea

ARTICLE INFO

Article history:
Received 30 November 2011
Received in revised form 16 April 2012
Accepted 20 April 2012
Available online 27 April 2012

Keywords:
Dye-sensitized solar cells (DSSCs)
Organic dyes
Phenanthroimidazole
Squaraine dye

ABSTRACT

Five functionalized organic dyes (H6-10) containing a phenanthroimidazole unit as an electron donor were synthesized and characterized for use in dye-sensitized solar cell (DSSC) applications. Under standard global AM 1.5 solar conditions, the DSSCs based on dye H6 displayed the best performance, with an incident photon-to-current conversion efficiency (IPCE) exceeding 70% at wavelengths of 400–530 nm, a short-circuit photocurrent density of 10.98 mA cm^{-2}, an open-circuit voltage of 0.68 V, a fill factor of 0.69, and an overall conversion efficiency of 5.12%. This efficiency is ~94% of that for JK2 cells (5.46%) and ~72% of that for N719 cells (7.07%) under the same conditions.

1. Introduction

In recent years, remarkable increases in energy consumption have led to a focus on renewable natural energy sources. The conversion of solar energy to electrical energy is very attractive, as sunlight is a clean and readily available resource. Since the first report in 1991 by Michael Grätzel et al., dye-sensitized solar cells (DSSCs) have received much attention because of their low production cost and relatively high energy conversion efficiency.[1] Compared with traditional silicon-based solar cells, DSSCs offer various advantages including cost effectiveness, tunability of the absorption region, and effective performance under diffuse light. Conventional DSSCs typically consist of a nanocrystalline titanium oxide, a sensitizer, and an electrolyte. Among these three parts, a suitable photosensitizer is essential in realizing highly efficient DSSCs. To date, ruthenium-based dyes have achieved high power conversion efficiencies of upto ~11%.[2] As an alternative to the commonly used ruthenium dyes, organic dyes have a variety of advantages, such as high molar extinction coefficients, easy modification of molecular structures, relatively low material costs and environmental friendliness.[3] Remarkable advances have been achieved in metal-free organic dyes, and recently, an impressive power conversion efficiency of over 10% has been reported.[4] As a key factor in the fabrication of highly efficient solar cells, a dye should possess several properties, including a wide absorption overlap with the solar spectrum for efficient light harvesting, appropriate HOMO and LUMO energy levels for efficient electron injection from the excited dye to the conduction band of TiO_2, rapid dye regeneration by electron injection into the oxidized dye from the redox couple, and hydrophobicity to minimize charge recombination.[5]

The general configuration of most reported organic dyes is a D-π-A structure because of its effective photoinduced intramolecular charge transfer (ICT) properties. The photophysical and electrochemical properties of such dyes can easily be tuned by incorporating a variety of donor, spacer, and acceptor moieties.[6] The most common donors used are arylamines, such as triphenylamine and carbazole, which are well known for their strong electron-donating and hole-transporting abilities.[7] In a recent study, imidazole-based donors, such as phenanthroimidazole and pyrenoimidazole also exhibited good electron-donating abilities.[8] The π-conjugated bridges often consist of thiophene or benzene units, and the acceptor is usually a cyanoacrylate group.[9]

Herein, we report the synthesis and DSSC performance of five functionalized organic dyes with D-π-A structures consisting of phenanthroimidazole as an electron donor and cyanoacetic acid as an anchoring group, which are linked by π-conjugated bridges, such as phenylene and thiophenylene moieties. A systematic investigation was performed to determine the effect of the number of phenylene on π-conjugated bridges (H6, H7, and H8). Moreover, we studied an influence of the N-functionalized group in the phenanthroimidazole

* Corresponding authors. Tel.: +82 2 880 6682; fax: +82 2 889 1568 (J.-I.H.); tel.: +82 41 860 1337; fax: +82 41 860 5396 (J.K.); e-mail addresses: jko@korea.ac.kr (J. Ko), jihong@snu.ac.kr (J.-I. Hong).

0040-4020/$ – see front matter © 2012 Elsevier Ltd. All rights reserved.
doi:10.1016/j.tet.2012.04.074

moiety, such as a tri(ethylene oxide) chain and a squaraine unit (H9 and H10). A tri(ethylene oxide) chain that coordinates Li^+ was introduced instead of n-butyl to retard charge recombination.[10] In an effort to realize panchromatic dyes, we combined an additional squaraine dye with the donor moiety to extend the absorption range to the near-IR region.[11] The overall conversion efficiencies of the devices sensitized with H6, H7, H8, H9 and H10 were 5.12%, 4.15%, 3.49%, 4.22%, and 2.18%, respectively.

2. Results and discussion

2.1. Synthesis

The molecular structures and the synthetic routes for the five dyes are illustrated in Schemes 1 and 2, respectively. 4-(2-(2-(2-methoxyethoxy)ethoxy)ethoxy)benzenamine **10**[12a] and (*E*)-3-hydroxy-4-((1,3,3-trimethylindolin-2-ylidene)methyl)cyclobut-3-ene-1,2-dione **14**[12b] and 5′-(4-bromophenyl)-[2,2′-bithiophene]-5-carbaldehyde **7**[12c] were synthesized as described in previous reports. The phenanthroimidazole donor parts were synthesized by the condensation of 9,10-phenanthrenequinone, aldehydes and arylamines (4-butylaniline, **10**, **16**) in the presence of ammonium acetate in acetic acid. The formylated compounds **3**, **8**, **9**, **13**, and **18** were then prepared by the palladium-catalyzed Stille reaction and the Suzuki reaction. Finally, Knoevenagel condensation reactions between the formylated compounds and cyanoacetic acid in the presence of piperidine provided the dyes, **H6**–**H10**. The details are illustrated in the experimental section.

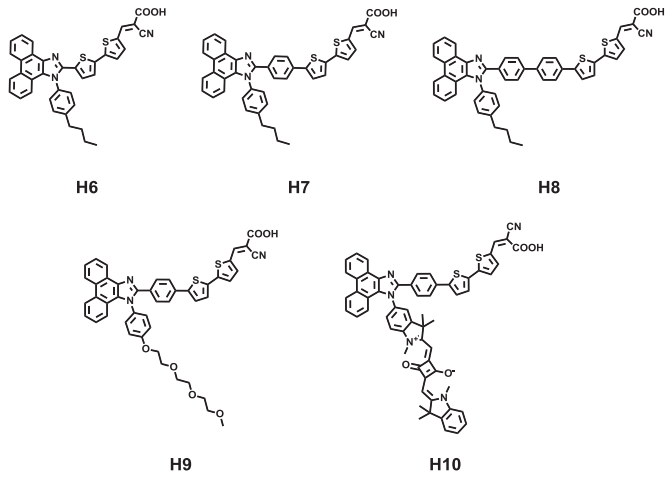

Scheme 1. Structures of dyes.

2.2. Photophysical properties

The UV-visible absorption spectra of the dyes in *N*,*N*-dimethylformamide (DMF) are shown in Fig. 1, and their photophysical data are listed in Table 1. All dyes possess distinct absorption bands in the visible region (350–500 nm) that are attributed to both the π–π^* transition of the conjugated system and an intramolecular charge transfer (ICT) transition from the phenanthroimidazole donor to the anchoring group. Interestingly, the absorption maximum peak of H6 (λ_{max}=432 nm) appears in the red-shifted region compared with that of H8 (λ_{max}=369 nm), which has two phenyl groups in the bridging unit (see Fig. 1). This phenomenon is in accord with the calculated geometric structure of the molecule (see Fig. 2).

A more planar structure can be achieved in H6, which does not have a biphenyl ring in the bridging unit, because the two adjacent phenyl groups are rather twisted, not only with respect to each other, but also with the adjacent phenanthroimidazole and thiophene moieties.[13] Thus, intramolecular charge transfer in H6 dye is more effective, leading to a bathochromic shift and the highest molar extinction coefficient among these three dyes (H6–8). Thus, the addition of phenyl rings did not contribute to extending the conjugation length and did not improve light-harvesting ability. In addition, H9 shows an absorption maximum (λ_{max}) at 420 nm, which is similar to that of H7 (λ_{max}=421 nm). However, the molar extinction coefficient of H9 (ε=46,655 M^{-1} cm^{-1}) is higher than that of H7 (ε=34,090 M^{-1} cm^{-1}).

Squaraines are dyes well known for their strong absorption in the near-IR region.[14] Despite their intense absorption, their spectral bands are located in a narrow region, limiting the efficiency of DSSC devices sensitized with squaraine dyes.[11,15] In recent years, squaraine units have been incorporated into the main conjugated backbone of dyes in efforts to extend their absorption range into the far-red region for panchromatic absorption. H10 displays two absorption maxima at 425 nm (ε=41,495 M^{-1} cm^{-1}) and 641 nm (ε=91,030 M^{-1} cm^{-1}), which are assigned to the main conjugated system and squaraine, respectively. Therefore, H10 seems to be a promising dye because its absorption range extends into the near-IR region.

The absorption spectra of dyes attached to the TiO_2 films display broader responses than those in solution (see Fig. 1b). The maximum absorption peaks of H6–H8, which all have a butylphenyl unit in the phenanthroimidazole moiety, are red-shifted in TiO_2 films, whereas those of H9 and H10 in TiO_2 films show slight blue-shifting compared with their absorption spectra in DMF solution. We presumed that these shifts in absorption spectra were caused by dye aggregation on the TiO_2 films.[16] It is worth noting that the broadening of absorption bands and longer tailing upon dye adsorption are advantageous for device performance.

2.3. Theoretical calculations

To achieve a better understanding of the molecular geometries and electronic distributions of the dyes, we performed density functional theory (DFT) calculations using the DFT B3LYP/6–31G(d) basis set in the Gaussian 09 software package. The electronic distributions and optimized geometries of the dyes are shown in Figs. 2and 3 and S2. In the case of the H6–H9 dyes, a butyl group was removed with ignorable effects on the molecular geometries and electronic distributions of the dyes. For the H6–H8 dyes, the HOMOs are mainly localized in the phenanthroimidazole unit and extend to the π-conjugated bridges and the LUMOs are located mainly over the cyanoacrylic moiety and also extend to the π-conjugated bridges. H6 has an almost planar conformation, whereas the phenyl groups in H7 and H8 result in an overall non-planar conformation. The calculated dihedral angles between phenanthroimidazole and the adjacent phenyl ring are 26.88° and 23.57° for H7 and H8, respectively. Additionally, the adjacent phenyl rings of H8 are more twisted, at 34.19° (Fig. 2). The torsion angles between the phenyl rings and thiophene are 23.41° and 17.87° for H7 and H8, respectively (Fig. 2). Therefore, π-electrons are more delocalized with fewer phenyl rings in the bridging part, which results in more effective π-conjugation. The twisted molecular geometries have negative effects on the light absorption region and photoinduced charge transfer, which results in the decreased photocurrent. Unlike the other dyes, in the case of H10, the HOMO is distributed over the squaraine unit, and HOMO-1 is populated in the phenanthroimidazole unit (Fig. 3). Moreover, the squaraine moiety is almost perpendicular to the phenanthroimidazole unit (82.58°), which is reflected in two independent

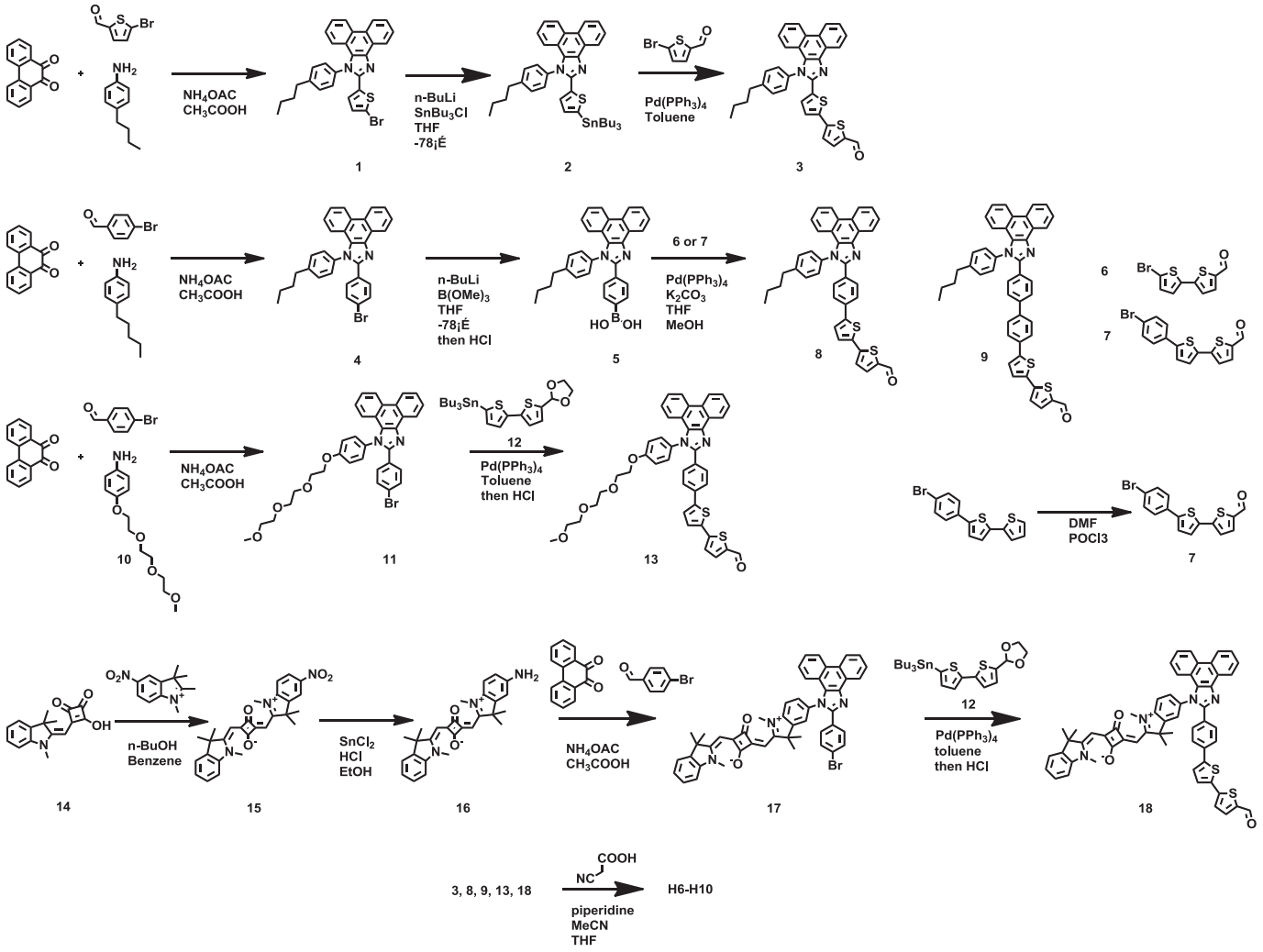

Scheme 2. Synthetic routes of dyes.

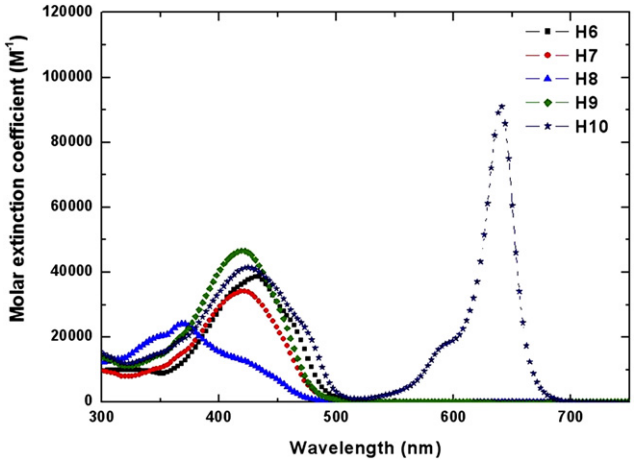

Fig. 1. Absorption spectra of dyes in 0.02 μM DMF solution.

light absorption regions (Fig. 1). This molecular geometry has a direct effect on cell performance, as discussed in the following section. In all the dyes, the LUMO is located over the conjugated bridges through cyanoacrylic acid. The apparent charge migration from the HOMO to the LUMO reveals that intramolecular charge transfer can occur except H10.

Table 1
Photophysical and electrochemical parameters of the dyes

Dyes	λ_{max} (ε)[a]/nm	E_{ox}[b]/V	E_{0-0}[c]/V	E^{*}_{0-0}[d]/V	HOMO[e]/eV	LUMO[e]/eV
H6	432 (38,625)	1.15	2.53	−1.38	5.31	2.78
H7	421 (34,090)	1.14	2.58	−1.44	5.30	2.72
H8	369 (24,275)	1.14	2.65	−1.51	5.30	2.65
H9	420 (46,655)	1.13	2.58	−1.45	5.29	2.71
H10	425 (41,495)	0.72	1.85	−1.13	4.88	3.03
	641 (91,030)					

[a] Maximum absorption spectra of dyes in DMF solution (2.0×10^{-5} M).
[b] Measured in DMF with 0.1 M $TBAPF_6$. The oxidation potential was determined from the onset of cyclic voltammograms with a scan rate of 100 mV s^{-1}. Potentials are calibrated with the internal ferrocene/ferrocenium (Fc/Fc^{+}) standard.
[c] E_{0-0} were derived from the 10% intensity of the absorption spectra.
[d] Calculated by $E^{*}_{0-0}=E_{ox.}-E_{0-0}$.
[e] Calculated based on $E_{HOMO}(Fc/Fc^{+})=4.8$ eV versus vacuum.

2.4. Electrochemical properties

To confirm the successful operation of DSSCs using the novel dyes H6–H10, the electrochemical properties of the dyes were determined by cyclic voltammetry (CV) in DMF using tetrabutylammonium hexafluorophosphate ($TBAPF_6$) as a supporting electrolyte; the data are summarized in Table 1. The first oxidation potentials (E_{ox}) of H6–H9 are in the range of 1.13–1.15 V versus the normal hydrogen electrode (NHE), which indicates that these four

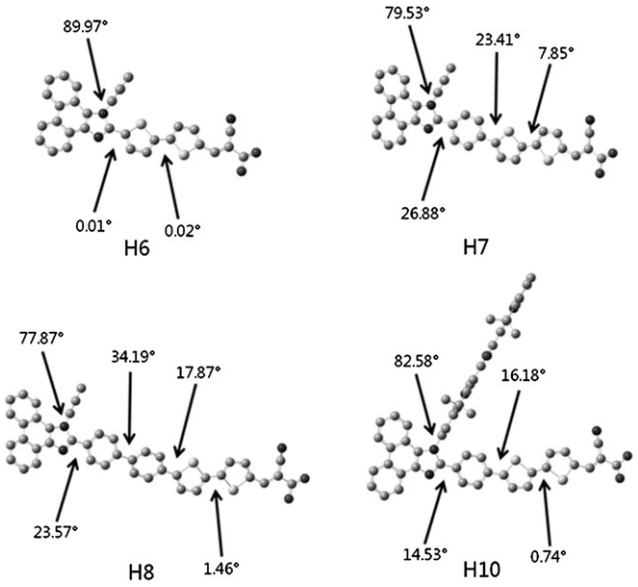

Fig. 2. Dihedral angles between aromatic rings of H dyes.

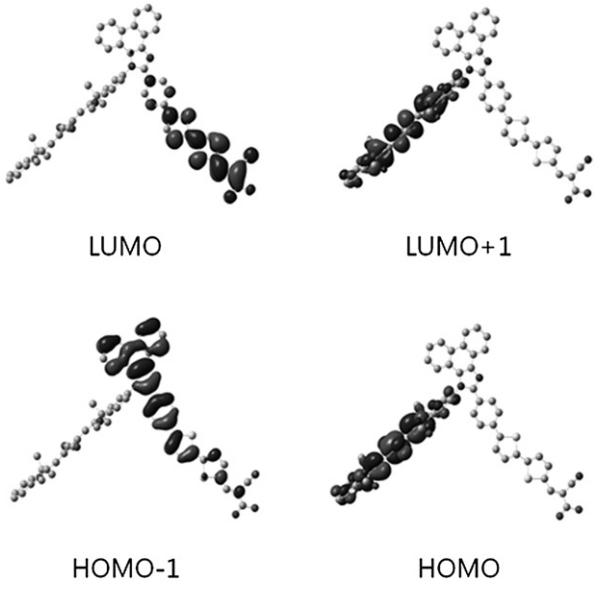

Fig. 3. Frontier molecular orbitals of H10 dye.

dyes have very similar HOMO energy levels. Our calculations indicated that the HOMOs of these dyes are mainly located in the phenanthroimidazole unit. However, the first oxidation peak of H10 was measured at 0.72 V, which is more negative than the others. This behavior corresponds to a different electronic distribution in the HOMO level of H10. All the calculated HOMO levels are sufficiently more positive than the I^-/I_3^- redox potential (E_{redox}=~0.4 V vs NHE), indicating that the regeneration of oxidized dyes from electrolytes is energetically favorable. The excited-state potentials (E^*_{0-0}) were calculated from the equation ($E^*_{0-0}=E_{ox.}-E_{0-0}$), where E_{0-0} is the zero–zero excitation energy derived from the wavelength at an intensity of 10% of the normalized absorption spectrum. In contrast to the similar HOMO levels of H6–H9, the LUMO energy values calculated from $E_{0\text{-}0}{}^*$ differ depending on the conjugated components in their bridges. Thus, H7 and H9 have similar HOMO and LUMO values because these two dyes have the same main π-conjugated system. However, H10 has the most positive LUMO level because it has a narrow band gap owing to the presence of the squaraine unit. The estimated LUMO levels of dyes are more negative than the conduction band edge of TiO_2 (E_{CB}=−0.5 V vs NHE),[17] indicating successful electron injection from the dyes into TiO_2. All the dyes have energetic configurations suitable for application as DSSC sensitizers.

2.5. Photovoltaic performance

Devices with TiO_2 layers of varying thicknesses were manufactured to optimize cell performance, and the most effective thickness was found to be 7 μm with a 4 μm scattering layer for all dyes. The liquid electrolyte was composed of 0.6 M 1,2-dimethyl-*n*-propylimidazolium iodide (DMPImI), 0.1 M LiI, 0.05 M I_2, and 0.5 M 4-*tert*-butylpyridine (TBP) in acetonitrile. Current density-voltage (*I*–*V*) characteristics and the incident photon-to-current conversion efficiency (IPCE) spectra were measured with a black tape mask under standard global AM 1.5 solar conditions (see Fig. 4 and Table 2). The H6-sensitized cell showed the best performance, with a short-circuit photocurrent density (J_{sc}) of 10.98 mA/cm^2, an open-circuit voltage (V_{oc}) of 0.68 V, and a fill factor (FF) of 0.68, yielding an overall cell efficiency (η) of 5.12% (see Table 2). For a precise comparison, JK2- and N719-sensitized cells were also fabricated under the same conditions; performance tests of these cells resulted in the following respective values: J_{sc}, 13.28 and 13.64 mA/cm^2; V_{oc}, 0.64 and 0.74 V; FF, 0.64 and 0.70; and η, 5.46 and 7.07%. The efficiency of the H6-based cell thus reached ~94% of that of the JK2 cell and ~72% of the N719 cell, indicating that the phenanthroimidazole unit is an efficient electron donor. The short-circuit photocurrent density increased in the order H8<H7<H6 because of the better light-harvesting ability of H6 than H7 and H8. The

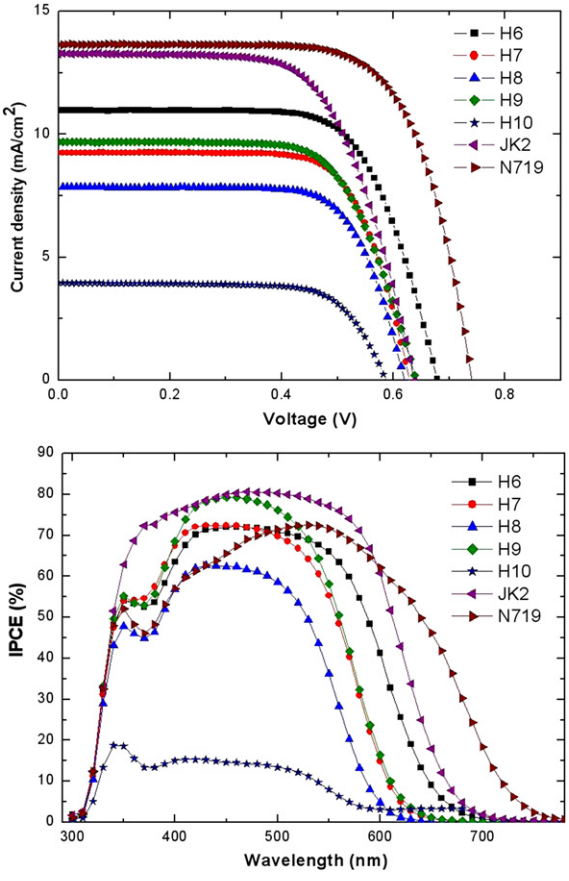

Fig. 4. *I*–*V* curve (top) and IPCE plot (bottom) of DSCs based on H dyes.

Table 2
Photovoltaic parameters of DSSCs based on the dyes in full sunlight (AM 1.5 G, 100 mW cm^{-2})

Dyes[a]	V_{oc} (V)	J_{sc} (mA/cm^2)	ff	η (%)
H6	0.68	10.98	68.64	5.12
H7	0.63	9.24	71.40	4.15
H8	0.62	7.85	71.67	3.49
H9	0.64	9.70	67.90	4.22
H10	0.59	3.95	71.52	1.66
JK2	0.64	13.28	64.45	5.46
N719	0.74	13.64	70.01	7.07

[a] Electrolyte composition : 0.6 M DMPIml, 0.1 M LiI, 0.05 M I_2, and 0.5 M TBP in acetonitrile.

relatively low efficiencies of H7 and H8 arise from their twisted molecular structures, which inhibit efficient ICT. H9 exhibits better photovoltaic performance than H7 because of the presence of a tri(ethylene oxide) chain instead of a butyl group. It has been clearly demonstrated that the tri(ethylene oxide) unit can coordinate Li^+.[10] The presence of lithium cations in the liquid electrolyte leads to a positive shift in the TiO_2 conduction band, causing a reduction in V_{oc}.[18] Incorporating tri(ethylene oxide) into the sensitizer thus enables the spatial separation of Li^+ from the TiO_2 surface as well as the high molecular extinction coefficient. Therefore, the Li^+ coordinating property of H9 positively affects both V_{oc} and J_{sc}. The device based on H10 showed a low efficiency of 1.66% because of its remarkable decrease in J_{sc} from that of H7 (3.95 vs 9.24 mA/cm^2). To elucidate the functional role of the tri(ethylene oxide) unit in the device performance of the H9-based cell, we performed electrochemical impedance spectroscopy (EIS) analysis.[12c] This method is generally used to investigate electron life time and charge recombination rate under open-circuit and dark conditions.[19] The second semicircle of the Nyquist plot (Fig. S4) is related to the charge recombination process. As shown in Fig. S4, the second semicircle radius decreases as going from H9 (10.8 Ω) to H7 (4.49 Ω), indicating that H9 more inhibits electron recombination from injected electrons in TiO_2 to electrolyte when compared with H7. Moreover, in the Bode phase plot (Fig. S4), the middle-frequency peak (in the 10–100 Hz range) is related to the life time of injected electrons in TiO_2 and is ultimately correlated with V_{oc}. The electron life time is obtained from the middle-frequency peak in the Bode phase plot using equation (1), where f is the frequency of the peak.

$$\tau = 1/2\pi f \quad (1)$$

The electron life time of H9 (7.33 ms) is longer than H7 (3.29 ms). This result is correlated with the fact that H9, which incorporates a tri(ethylene oxide) unit, has slightly higher V_{oc} and J_{sc} values than H7. Thus, the presence of the tri(ethylene oxide) in the H9 dye as a functional unit suppress charge recombination, which ultimately contributes to the positive effect on the photoconversion efficiency.

Although H10 showed the widest photo-active region from 350 to 700 nm, the device based on H10 exhibited the lowest photocurrent of 3.95 mA/cm^2 as well as only ~19% of the maximum IPCE. There are two reasons for poor performance of the H10-based device: (1) inefficient charge transfer from the squaraine unit to the main conjugated system and (2) Förster resonance energy transfer (FRET) from the main conjugated system to the squaraine unit. First, the low efficiency of the H10-based cell arises from an unfavorable charge transfer from the squaraine moiety to the phenanthroimidazole unit, which is caused by the perpendicular molecular geometry between squaraine and phenanthroimidazole (see Fig. 2), despite the improved light-harvesting ability of H10. This speculation is supported by low IPCE at>600 nm in the squaraine absorption region (Fig. 4). The injection of electrons generated by the squaraine unit into the TiO_2 conduction band via the anchoring group is unfavorable. Second, as shown in Fig. 4, H10 shows very low photon-to-current conversion efficiency below 20% in the 400–600 nm region. We measured photoluminescence (PL) spectra of a squaraine derivative (sq, Scheme S1), H7 and H10 dyes in 1 mM DMF solution (see Fig. 5).[14] H7 and sq exhibit maximum emissions at 556 nm (ex. 450 nm) and 688 nm (both ex. 450 nm and 556 nm), respectively. When the main conjugated system of H10 is excited at 450 nm, only one emission peak is observed, which mostly comes from the squaraine moiety (λ_{max}=704 nm). This indicates that emission of H10 arises from the Förster resonance energy transfer from the main conjugated system to the squaraine moiety. To confirm the FRET in H10, we prepared a blending solution of H7 and sq (1:1) and measured its PL spectrum. As shown in Fig. 5, the maximum PL of the blending solution was observed at 684 nm (ex. 450 nm). This emission profile is similar to that of H10. Consequently, as H10 dye absorbs whole region from UV–vis to NIR, two processes are operative: intramolecular FRET from the main conjugated system to the squaraine unit and inefficient charge transfer to the TiO_2 conduction band through the phenanthroimidazole group, which induce the low photoconversion efficiency. In contrast with H10, other H dyes possess IPCE spectra ranging from 300 to 700 nm, exceeding 60% in the range of 400–500 nm. Especially, H9 exhibits a maximum value close to 80%, which is ascribed to its highest molar extinction coefficient. This is because the perpendicular molecular geometry between squaraine and phenanthroimidazole causes an unfavorable charge transfer from the squaraine moiety to the phenanthroimidazole unit (see Fig. 2), despite the improved light harvesting ability of H10. This interpretation is supported by the incident photon-to-current conversion efficiency (IPCE) spectra shown in Fig. 4.

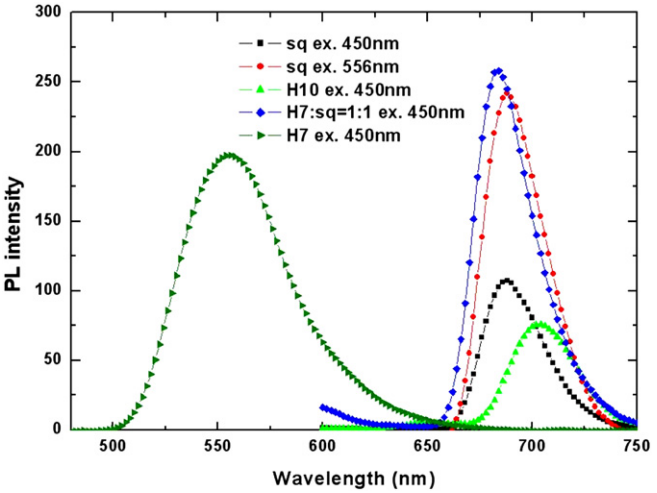

Fig. 5. Photoluminescent spectra of sq, H7 and H10 in DMF solution.

3. Conclusion

We synthesized five functionalized organic dyes containing a phenanthroimidazole donor for use in dye-sensitized solar cells. The best performance was obtained with the H6 dye, yielding an efficiency of 5.12%, which is comparable to the reference cell based on JK-2 (5.46%), suggesting that phenanthroimidazole is a promising electron donor. The photovoltaic performance of dyes improved with a decrease in the number of phenyl rings because the large dihedral angle between aromatic rings in the bridges has a negative effect on intramolecular charge transfer. The H9-sensitized DSSC

exhibited slightly better photovoltaic performance than that of H7 because the tri(ethylene oxide) chain in H9 can coordinate with Li^+ and thus retard charge recombination. The H10 dye, containing an extra squaraine moiety, was synthesized to extend the absorption range into the near-IR region. Although H10 has an intense absorption band from 300 to 700 nm, low efficiency was observed because of unfavorable electron transfer to the conduction band of TiO_2 and FRET from the main conjugated system to the squaraine unit. Our results show that the coplanar geometry and suitable energy levels should be carefully considered in designing new dyes. It is very clear that photovoltaic dye performance is significantly affected by the conjugated components and functionalized moieties.

4. Experimental

4.1. General information

All organic chemicals were purchased from Aldrich and TCI. Column chromatography was performed on Merck silica gel 60 (70–230 mesh). All solvents and reagents were commercially available and used without further purification unless otherwise noted. Melting points were measured using Electrothermal 9100 from BARNSTEAD. ^1H and ^{13}C NMR spectra were recorded using an Advance 300 or 500 MHz Bruker spectrometer. ATR-FTIR spectra were obtained using Nicolet iS10 FTIR spectrometer from ThermoFisher. UV–vis spectra were recorded on a Beckman DU 650 spectrophotometer. Mass spectra were obtained using a Gas Chromatography-Mass Spectrometer from JEOL, JMS-AX505WA, HP 5890 Series II and a MALDI-TOF MS from Bruker. Cyclic voltammetry (CV) was performed using a CH Instruments 660 Electrochemical Analyzer (CH Instruments, Inc., Texas) with a 0.1 M tetra-*n*-butylammonium hexafluorophosphate (Bu_4NPF_6) in DMF solution as the supporting electrolyte at room temperature. The CV was recorded using an Ag/Ag^+ reference electrode (0.1 M $AgNO_3$ in acetonitrile) with a platinum wire counterelectrode at a scan rate of 100 mV s^{-1}. The ferrocene/ferrocenium redox couple was calibrated to a normal hydrogen electrode (NHE). The theoretical energy levels of the dyes were obtained by density functional theory (DFT) calculations at the B3LYP/6–31G(d) level with the Gaussian 09 program. The photovoltaic performances of the DSSCs were measured using a 1000-W xenon light source, with power calibration as an AM 1.5 Oriel solar simulator using a KG5-filtered Si reference solar cell. The IPCE spectra for the cells were measured on an IPCE measuring system (PV Measurements).

4.2. Synthetic procedures and characterizations

*4.2.1. 2-(5-Bromothiophen-2-yl)-1-(4-butylphenyl)-1H-phenanthro[9,10-d]imidazole (**1**).* A mixture of 9,10-phenanthrenequinone (1 g, 4.8 mmol), 5-bromo-2-thiophenecarboxaldehyde (0.571 mL, 4.8 mmol), 4-butylaniline (3.79 mL, 24 mmol), ammonium acetate (1.48 g, 19.2 mmol), and glacial acetic acid (40 mL) was refluxed for 3 h. After cooling to room temperature, water was added. The precipitate was collected via filtration, and washed with water and methanol to give a pale brown solid (yield: 1.061 g, 43%). Mp 166 °C; ^1H NMR (300 MHz, DMSO-d_6): δ (ppm) 8.92–8.89 (d, J=8.4 Hz, 1H), 8.87–8.84 (d, J=8.3 Hz, 1H), 8.62–8.60 (d, J=7 Hz, 1H), 7.79–7.52 (m, 7H), 7.34–7.29 (t, J=7.7 Hz, 1H), 7.14–7.13 (d, J=4 Hz, 1H), 7.10–7.07 (d, J=8 Hz, 1H), 6.59–6.58 (d, J=4 Hz, 1H), 2.87–2.82 (t, J=7.4 Hz, 2H), 1.75–1.70 (t, J=7.4 Hz, 2H), 1.43–1.36 (q, J=7.4 Hz, 2H), 1.00–0.95 (t, J=7.3 Hz, 3H); ^{13}C NMR (75 MHz, $CDCl_3$): δ (ppm) 151.6, 146.0, 145.1, 137.4, 135.4, 134.7, 130.7, 130.2, 129.3, 128.9, 128.3, 128.3, 127.3, 126.9, 126.4, 125.7, 125.0, 124.1, 123.1, 122.8, 120.6, 114.8, 35.5, 33.4, 22.2, 14.0; ATR-FTIR (KBr, cm^{-1}): 3032, 3053, 2952, 2929, 2867, 1612, 1516, 1473, 1453, 1235, 1036, 848, 781, 747, 719; MALDI-TOF MS, m/z: calcd for $C_{29}H_{23}BrN_2S$: 510.077, found: 510.799 $[M]^+$.

*4.2.2. 2-(4-Bromophenyl)-1-(4-butylphenyl)-1H-phenanthro[9,10-d]imidazole (**4**).* Compound **4** was prepared according to the synthetic procedure for compound **1**, using 4-bromobenzaldehyde instead of 5-bromo-2-thiophenecarboxaldehyde (yield: 67%). Mp 168 °C; ^1H NMR (300 MHz, $CDCl_3$): δ (ppm) 8.89–8.86 (d, J=7.8 Hz, 1H), 8.78–8.76 (d, J=8.4 Hz, 1H), 8.72–8.70 (d, J=8.3 Hz, 1H), 7.78–7.74 (t, J=7.1 Hz, 1H), 7.69–7.64 (t, J=8.3 Hz, 1H), 7.55–7.37 (m, 9H), 7.28–7.20 (m, 2H), 2.85–2.80 (t, J=7.6 Hz, 2H), 1.79–1.74 (t, J=7.7 Hz, 2H), 1.50–1.43 (q, J=7.5 Hz, 2H), 1.07–1.02 (t, J=7.3 Hz, 3H); ^{13}C NMR (75 MHz, $CDCl_3$): δ (ppm) 149.7, 145.1, 137.4, 135.9, 131.4, 130.8, 130.2, 129.6, 129.3, 128.7, 128.4, 128.3, 127.3, 127.2, 126.3, 125.7, 124.9, 124.1, 123.3, 123.1, 123.0, 122.7, 120.9, 35.4, 33.3, 22.3, 14.0; ATR-FTIR (KBr, cm^{-1}): 3064, 2955, 2918, 2854, 1606, 1575, 1511, 1463, 1450, 1008, 829, 798, 752, 723; MALDI-TOF MS, m/z: calcd for $C_{31}H_{25}BrN_2S$: 504.120, found: 504.172 $[M]^+$.

*4.2.3. 2-(4-Bromophenyl)-1-(4-(2-(2-(2-methoxyethoxy)ethoxy)ethoxy)phenyl)-1H-phenanthro[9,10-d]imidazole (**11**).* Compound **11** was prepared according to the synthetic procedure for compound **4**, using **10**[12a] instead of 4-butylaniline. The crude product was further purified by silica gel column chromatography using CH_2Cl_2/EtOAC (10:1) as an eluent to give a pale brown solid (yield: 89%). Mp 119 °C; ^1H NMR (300 MHz, $CDCl_3$): δ (ppm) 8.86–8.83 (d, J=8.1 Hz, 1H), 8.78–8.76 (d, J=8.4 Hz, 1H), 8.72–8.69 (d, J=8.1 Hz, 1H), 7.77–7.72 (t, J=7.7 Hz, 1H), 7.68–7.63 (m, 1H), 7.56–7.43 (m, 5H), 7.41–7.38 (d, J=8.8 Hz, 2H), 7.34–7.24 (m, 2H), 7.13–7.10 (d, J=8.8 Hz, 2H), 4.29–4.26 (t, J=4.3 Hz, 2H), 3.99–3.96 (t, J=4.8 Hz, 2H), 3.84–3.81 (m, 2H), 3.77–3.65 (m, 4H), 3.61–3.58 (m, 2H), 3.41 (s, 3H); ^{13}C NMR (75 MHz, $CDCl_3$): 159.6, 149.8, 137.2, 131.4, 131.0, 130.7, 129.8, 129.4, 129.2, 128.4, 128.2, 127.2, 127.1, 126.4, 125.6, 125.0, 124.0, 123.2, 123.1, 123.0, 122.6, 120.8, 115.9, 71.9, 70.9, 70.6, 70.6, 69.6, 67.8, 59.1; ATR-FTIR (KBr, cm^{-1}): 3037, 2985, 2880, 2861, 1608, 1508, 1449, 1247, 1107, 1062, 1007, 828, 757, 726; MALDI-TOF MS, m/z: calcd for $C_{34}H_{31}$ BrN_2O_4: 610.147, found: 610.829 $[M]^+$.

*4.2.4. (Z)-4-((5-(2-(4-bromophenyl)-1H-phenanthr-o[9,10-d]imidazol-1-yl)-1,3,3-trimethyl-3H-indolium-2-yl)methylene)-3-oxo-2-((Z)-(1,3,3-trimethylindolin-2-ylidene)methyl)cyclobut-1-enolate (**17**).* Compound **17** was prepared according to the synthetic procedure for compound **4**, using **16** instead of 4-butylaniline. The crude product was further purified by silica gel column chromatography using EtOAC/methanol (10:1) as an eluent to give a greenish-blue solid (yield: 74%). Mp 279 °C; ^1H NMR (300 MHz, $CDCl_3$): δ (ppm) 8.86–8.83 (d, J=7.9 Hz, 1H), 8.80–8.77 (d, J=8.5 Hz, 1H), 8.73–8.70 (d, J=8.3 Hz, 1H), 7.78–7.73 (t, J=7.1 Hz, 1H), 7.70–7.64 (t, J=8.1 Hz, 1H), 7.55–7.19 (m, 12H), 7.09–7.06 (d, J=7.9 Hz, 2H), 6.01 (s, 2H), 3.64 (s, 3H), 3.59 (s, 3H), 1.84 (s, 6H), 1.80 (s, 6H); ^{13}C NMR (75 MHz, $CDCl_3$): δ (ppm) 182.2, 177.03, 173.2, 168.3, 149.2, 142.3, 142.0, 131.8, 131.6, 131.1, 129.5, 128.4, 128.0, 127.8, 127.7, 127.2, 126.6, 126.4, 125.7, 125.4, 124.8, 124.4, 124.2, 123.1, 123.0, 122.7, 122.3, 122.2, 120.8, 110.0, 109.8, 87.9, 87.7, 49.8, 48.5, 31.3, 30.7, 29.7, 27.2, 26.7; ATR-FTIR (KBr, cm^{-1}): 3070, 2960, 2927, 1738, 1601, 1505, 1481, 1459, 1426, 1271, 1347, 1222, 1097, 1067, 965, 922, 806, 789, 754; MALDI-TOF MS, m/z: calcd for $C_{49}H_{39}BrN_4O_2$: 794.226, found: 794.818 $[M]^+$.

*4.2.5. 1-(4-Butylphenyl)-2-(5-(tributylstannyl)thiophen-2-yl)-1H-phenanthro[9,10-d]imidazole (**2**).* A solution of *n*-butyllithium (0.656 mL, 2.5 M in hexane, 1.64 mmol) was added dropwise to a cooled solution of **1** (0.7 g, 1.37 mmol) in dry THF (40 mL) at −78 °C under nitrogen. The reaction mixture was stirred at the same temperature for 1 h and treated with tributyltin chloride (0.922 mL, 3.42 mmol). The resulting mixture was allowed to attain room temperature and stirred overnight. After quenching with water, the

mixture was extracted with CH_2Cl_2. The organic layer was dried over Na_2SO_4 and concentrated in vacuo. The crude product was purified by silica gel column chromatography using CH_2Cl_2/hexane (1:5) as an eluent to give a pale brown solid (yield: 0.493 g, 50%). Mp 117 °C; ^{1}H NMR (500 MHz, $CDCl_3$): δ (ppm) 8.88–8.86 (m, 1H), 8.75–8.74 (d, *J*=8.3 Hz, 1H), 8.69–8.68 (d, *J*=8.4 Hz, 1H), 7.75–7.71 (m, 1H), 7.66–7.62 (m, 1H), 7.51–7.47 (m, 5H), 7.24–7.23 (m, 1H), 7.18–7.16 (d, *J*=8.3 Hz, 1H), 6.97–6.93 (m, 2H), 2.88–2.84 (m, 2H) 1.82–1.76 (m, 2H), 1.68–1.62 (m, 2H), 1.56–1.47 (m, 6H), 1.37–1.28 (m, 8H), 1.11–1.08 (m, 4H), 1.05–1.02 (m, 3H), 0.94–0.88 (m, 9H); ^{13}C NMR (75 MHz, $CDCl_3$): δ (ppm) 146.5, 145.5, 140.2, 138.6, 137.6, 136.0, 135.6, 130.4, 129.1, 129.0, 128.2, 128.1, 127.8, 127.1, 126.5, 125.5, 124.7, 124.0, 123.0, 120.6, 35.5, 33.5, 28.9, 27.6, 22.3, 14.0, 13.7, 10.8; ATR-FTIR (KBr, cm^{-1}): 3058, 2955, 2919, 1608, 1574, 1554, 1513, 1453, 1235, 1095, 838, 786, 751, 723; MALDI-TOF MS, *m*/*z*: calcd for $C_{41}H_{50}N_2SSn$: 722.272, found: 721.831 $[M]^+$.

*4.2.6. 4-(1-(4-Butylphenyl)-1H-phenanthro[9,10-d]-imidazol-2-yl) phenylboronic acid (**5**).* A solution of n-butyllithium (0.95 mL, 2.5 M in hexane, 2.38 mmol) was added dropwise to a cooled solution of **4** (1 g, 1.98 mmol) in dry THF (50 mL) at -78 °C under nitrogen. The reaction mixture was stirred at the same temperature for 1 h and treated with trimethylborate (0.331 mL, 2.97 mmol). The resulting mixture was allowed to attain room temperature and was stirred overnight. 1 N HCl solution was added, and the mixture was stirred for 3 h and then extracted with CH_2Cl_2. The organic layer was dried over Na_2SO_4 and concentrated in vacuo. The crude product was purified by silica gel column chromatography using CH_2Cl_2/methanol (1:10) as an eluent to give a white solid (yield: 0.466 g, 50%). Mp 185 °C; ^{1}H NMR (300 MHz, DMSO-d_6): 8.93–8.90 (d, *J*=8.4 Hz, 1H), 8.88–8.85 (d, *J*=8.3 Hz, 1H), 8.70–8.68 (d, *J*=7.4 Hz, 1H), 8.14 (s, 2H), 7.82–7.65 (m, 4H), 7.59–7.47 (m, 7H), 7.33–7.28 (t, *J*=7.7 Hz, 1H), 7.12–7.09 (t, *J*=8.5 Hz, 1H), 2.79–2.75 (t, *J*=7.5 Hz, 2H), 1.70–1.63 (t, *J*=7.4 Hz, 2H), 1.40–1.32 (q, *J*=7.3 Hz, 2H), 0.98–0.93 (t, *J*=7.2 Hz, 3H); ^{13}C NMR (75 MHz, DMSO-d_6): δ (ppm) 151.0, 145.0, 136.9, 126.2, 124.2, 132.1, 130.6, 129.3, 129.0, 128.4, 128.3, 128.1, 127.9, 127.2, 127.0, 126.2, 125.7, 124.9, 124.1, 123.0, 122.5, 122.4, 120.7, 34.9, 33.3, 22.0, 14.3; ATR-FTIR (KBr, cm^{-1}): 3058, 2955, 2925, 2856, 1608, 1514, 1342, 1278, 1018, 844, 753, 723; MALDI-TOF MS, *m*/*z*: calcd for $C_{31}H_{27}BN_2O_2$: 470.217, found: 471.245 $[M+H]^+$.

*4.2.7. 5′-(1-(4-Butylphenyl)-1H-phenanthro[9,10-d]imidazol-2-yl)-2,2′-bithiophene-5-carbaldehyde (**3**).* A mixture of **2** (0.493 g, 0.68 mmol), 5-bromo-2-thiophenecarboxaldehyde (0.081 mL, 0.68 mmol), and $Pd(PPh_3)_4$ (0.039 g, 0.034 mmol) in toluene (40 mL) was refluxed overnight under nitrogen. After cooling to room temperature, the reaction mixture was extracted with CH_2Cl_2 and the organic layer was dried over Na_2SO_4. The solvent was evaporated in vacuo to give the crude product, which was purified by silica gel column chromatography using CH_2Cl_2 as an eluent to give an orange solid (yield: 0.17 g, 46%). Mp 196 °C; ^{1}H NMR (300 MHz, $CDCl_3$): δ (ppm) 9.87 (s, 1H), 8.86–8.83 (d, *J*=7.4 Hz, 1H), 8.76–8.74 (d, *J*=8.4 Hz, 1H), 8.71–8.68 (d, *J*=8.2 Hz, 1H), 7.78–7.65 (m, 3H), 7.54–7.49 (m, 5H), 7.30–7.18 (m, 3H), 7.14–7.12 (d, *J*=4 Hz, 1H), 6.76–6.75 (d, *J*=4 Hz, 1H), 2.93–2.88 (t, *J*=7.5 Hz, 2H), 1.85–1.80 (t, *J*=7.7 Hz, 2H), 1.55–1.47 (q, *J*=7.5 Hz, 2H), 1.08–1.04 (t, *J*=7.3 Hz, 3H); ^{13}C NMR (75 MHz, $CDCl_3$): δ (ppm) 182.4, 146.4, 146.0, 144.9, 141.8, 137.2, 137.0, 135.4, 134.5, 130.7, 129.3, 128.8, 128.3, 128.3, 127.6, 127.2, 126.7, 126.3, 126.3, 125.8, 125.1, 124.4, 124.0, 123.1, 122.8, 122.7, 120.6, 35.5, 33.4, 22.2, 14.0; ATR-FTIR (KBr, cm^{-1}): 3035, 2952, 2926, 2855, 1653, 1575, 1515, 1451, 1230, 1051, 782, 746, 718; MALDI-TOF MS, *m*/*z*: calcd for $C_{34}H_{26}N_2OS_2$: 542.149, found: 542.850 $[M]^+$.

*4.2.8. 5′-(4-(1-(4-Butylphenyl)-1H-phenanthro[9,10-d]imidazol-2-yl)phenyl)-2,2′-bithiophene-5-carbaldehyde (**8**).* Compound **8** was prepared according to the synthetic procedure for compound **3**, using **5** and 5′-bromo-2,2′-bithio-phene-5-carbaldehyde instead of **2** and 5-bromo-2-thiophenecarboxaldehyde, respectively. The crude product was purified by silica gel column chromatography using CH_2Cl_2 as an eluent to give an orange solid. (yield: 56%). Mp 208 °C; ^{1}H NMR (300 MHz, DMSO-d_6): δ (ppm) 9.89 (s, 1H), 8.94–8.92 (d, *J*=8.4 Hz, 1H), 8.89–8.87 (d, *J*=8.4 Hz, 1H), 8.72–8.70 (d, *J*=7.8 Hz, 1H), 8.02–8.01 (d, *J*=4 Hz, 1H), 7.79–7.61(m, 11H), 7.59–7.58 (d, *J*=3.7 Hz, 1H), 7.56–7.50 (m, 2H), 7.34–7.29 (t, *J*=7.3 Hz, 1H), 7.11–7.08 (d, *J*=8.3 Hz, 1H), 2.82–2.77 (t, *J*=7 Hz, 2H), 1.72–1.67 (t, *J*=6.8 Hz, 2H), 1.40–1.33 (q, *J*=7.1 Hz, 2H), 0.98–0.93 (t, *J*=7.2 Hz, 3H); ^{13}C NMR (75 MHz, $CDCl_3$): δ (ppm) 182.4, 149.9, 146.9, 145.2, 145.0, 141.6, 137.4, 136.1, 135.4, 133.4, 130.2, 130.1, 129.7, 129.6, 129.3, 128.7, 128.4, 128.3, 127.3, 127.1, 126.6, 126.2, 125.6, 125.3, 124.9, 124.6, 124.1, 123.1, 123.0, 122.7, 120.9, 35.4, 33.3, 22.2, 14.0; ATR-FTIR (KBr, cm^{-1}): 3058, 2988, 2891, 2856, 1642, 1514, 1450, 1439, 1247, 1225, 1113, 1055, 794, 756, 723; MALDI-TOF MS, *m*/*z*: calcd for $C_{40}H_{30}N_2OS_2$: 618.180, found: 619.314 $[M+H]^+$.

*4.2.9. 5′-(4′-(1-(4-Butylphenyl)-1H-phenanthro[9,1-d]imidazol-2-yl) bi-phenyl-4-yl)-2,2′-bithiophene-5 -carbaldehyde (**9**).* Compound **9** was prepared according to the synthetic procedure for compound **8**, using **7**[12c] instead of **6**. The crude product was purified by silica gel column chromatography using CH_2Cl_2 as an eluent to give a yellow solid (yield: 61%). Mp 212 °C; ^{1}H NMR (300 MHz, DMSO-d_6): δ (ppm) 9.89 (s, 1H), 8.94–8.92 (d, *J*=8.4 Hz, 1H), 8.89–8.87 (d, *J*=8.3 Hz, 1H), 8.72–8.69 (d, *J*=7.9 Hz, 1H), 8.02–8.01 (d, *J*=4 Hz, 1H), 7.78–7.71 (t, *J*=7.5 Hz, 1H), 7.68–7.62 (m, 9H), 7.60–7.50 (m, 8H), 7.34–7.29 (d, *J*=7.3 Hz, 1H), 7.11–7.08 (d, *J*=8.3 Hz, 1H), 2.82–2.77 (t, *J*=8.8 Hz, 2H), 1.73–1.68 (t, *J*=7.6 Hz, 2H), 1.41–1.34 (q, *J*=7.4 Hz, 2H), 0.98–0.94 (t, *J*=7.3 Hz, 3H); ^{13}C NMR (75 MHz, $CDCl_3$): δ (ppm) 182.4, 150.3, 145.5, 144.9, 141.5, 140.2, 140.1, 139.9, 137.3, 136.2, 132.6, 130.1, 129.7, 129.6, 129.2, 128.7, 128.3, 128.2, 127.5, 127.2, 127.2, 126.6, 126.5, 126.2, 126.1, 125.9, 125.6, 125.4, 124.8, 124.2, 124.0, 123.9, 123.1, 122.7, 120.9, 35.4, 33.3, 22.2, 14.0; ATR-FTIR (KBr, cm^{-1}): 3057, 2954, 2924, 2854, 1660, 1514, 1452, 1226, 1145, 1046, 794, 752, 723; MALDI-TOF MS, *m*/*z*: calcd for $C_{46}H_{34}N_2OS_2$: 694.211, found: 695.405 $[M+H]^+$.

*4.2.10. 5′-(4-(1-(4-(2-(2-(2-Methoxyethoxy)ethoxy)-ethoxy)phenyl)-1H-phenanthro[9,10-d]imidazol-2-y-l)phenyl)-2,2′-bithiophene-5-carbaldehyde (**13**).* A mixture of **11** (0.556 g, 0.91 mmol), (5′-(1,3-dioxolan-2-yl)-2,2′-bithiophen-5-yl)tributylstannane[20a] **12** (0.96 g, 1.82 mmol), and $Pd(PPh_3)_4$ (0.053 g, 0.045 mmol) in toluene (40 mL) was refluxed overnight under nitrogen. After cooling to room temperature, a 1 N HCl solution was added, and the mixture was stirred for 3 h. The precipitate was collected via filtration to give the crude product, which was purified by silica gel column chromatography using CH_2Cl_2/EtOAC (5:1) as an eluent to give an orange solid (yield: 0.515 g, 78%). Mp 176 °C; ^{1}H NMR (500 MHz, DMSO-d_6): δ (ppm) 9.88 (s, 1H), 8.92–8.90 (d, *J*=8.5 Hz, 1H), 8.87–8.85 (d, *J*=8.5 Hz, 1H), 8.70–8.68 (d, *J*=7.9 Hz, 1H), 8.01–7.99 (d, *J*=4 Hz, 1H), 7.78–7.75 (t, *J*=7.1 Hz, 1H), 7.73–7.72 (d, *J*=8.3 Hz, 2H), 7.69–7.63 (m, 7H), 7.57–7.54 (m, 2H), 7.40–7.37 (t, *J*=7.9 Hz, 1H), 7.25–7.23 (d, *J*=8.7 Hz, 2H), 7.20–7.18 (d, *J*=8.3 Hz, 1H), 4.24–4.23 (t, *J*=4 Hz, 2H), 3.83–3.81 (t, *J*=4.4 Hz, 2H), 3.64–3.62 (m, 2H), 3.57–3.55 (m, 2H), 3.54–3.52 (m, 2H), 3.44–3.42 (m, 2H), 3.22 (s, 3H); ^{13}C NMR (75 MHz, $CDCl_3$): 184.3, 159.8, 151.4, 150.3, 145.6, 144.4, 141.8, 139.6, 136.9, 135.3, 133.4, 131.1, 130.6, 130.0, 129.0, 128.8, 128.6, 128.1, 127.9, 127.2, 127.1, 126.5, 126.2, 125.7, 125.7, 125.6, 124.9, 123.0, 122.4, 120.7, 116.4, 110.4, 71.7, 70.5, 70.3, 70.1, 69.4, 68.1, 58.5; ATR-FTIR (KBr, cm^{-1}): 3056, 2923, 2892, 2853, 1642, 1514, 1451,1247, 1225, 1113, 1055, 839, 794, 756, 723; MALDI-TOF MS, *m*/*z*: calcd for $C_{43}H_{36}N_2O_5S_2$: 724.207, found: 724.808 $[M]^+$.

4.2.11. (Z)-4-((5-(2-(4-(5′-Formyl-2,2′-bithiophen-5-yl)phenyl)-1H-phenanthro[9,10-d]imidazol-1-yl)-1,3,3-trimethyl-3H-indolium-2-yl) methylene)-3-oxo-2-((Z)-(1,3,3-trimethylindolin-2-ylidene)methyl)

*cyclobut-1-enolate (**18**).* Compound **18** was prepared according to the synthetic procedure for compound **13** using **17** instead of **11**. The crude product was purified by silica gel column chromatography using EtOAC/methanol (20:1) as an eluent to give a greenish-blue solid (yield: 37%). Mp 294 °C; ^{1}H NMR (500 MHz, $CDCl_3$): δ (ppm) 9.86 (s, 1H), 8.89–8.87 (d, J=7.9 Hz, 1H), 8.80–8.78 (d, J=8.4 Hz, 1H), 8.73–8.71 (d, J=8.3 Hz, 1H), 7.78–7.75 (t, J=7.1 Hz, 1H), 7.69–7.63 (m, 4H), 7.56–7.53 (m, 3H), 7.49 (s, 1H), 7.42–7.34 (m, 3H), 7.32–7.29 (m, 4H), 7.25–7.24 (d, J=3.9 Hz, 1H), 7.23–7.20 (t, J=7.5 Hz, 1H), 7.11–7.10 (d, J=8.2 Hz, 1H), 7.08–7.07 (d, J=7.9 Hz, 1H), 6.0 (s, 2H), 3.65 (s, 3H), 3.61 (s, 3H), 1.79 (s, 6H), 1.78 (s, 6H); ^{13}C NMR (75 MHz, $CDCl_3$): 183.1, 182.4, 178.3, 172.9, 168.5, 150.1, 146.8, 145.0, 144.1, 144.0, 142.6, 142.0, 141.6, 137.3, 135.6, 133.6, 133.1, 129.8, 129.4, 128.9, 128.4, 128.3, 128.2, 128.0, 127.4, 127.1, 126.9, 126.3, 125.8, 125.3, 125.1, 124.7, 124.2, 124.1, 123.1, 122.8, 122.3, 120.7, 109.8, 109.5, 87.8, 87.5, 49.8, 48.6, 31.2, 30.6, 27.3, 27.2, 26.8; ATR-FTIR (KBr, cm^{-1}): 3068, 2972, 2933, 1735, 1650, 1601, 1504, 1481, 1459, 1426, 1271, 1347, 1223, 1097, 1067, 965, 923, 806, 789, 754, 725; MALDI-TOF MS, m/z: calcd for $C_{58}H_{44}N_4O_3S_2$: 908.286, found: 908.843 $[M]^+$.

*4.2.12. (Z)-3-oxo-4-((1,3,3-Trimethyl-5-nitro-3H-indolium-2-yl) methylene)-2-((Z)-(1,3,3-trimethylindolin-2-ylidene)methyl)cyclobut-1-enolate (**15**).* (*E*)-3-Hydroxy-4-((1,3,3-trimethylindolin-2-ylidene)methyl)cyclobut-3-ene-1,2-dione **14**[12b] (0.713 g, 2.65 mmol) and 1,2,3,3-tetra methyl-5-nitro-3*H*-indolium iodide[20b] (1.21 g, 3.98 mmol) were dissolved in a mixture of benzene (10 mL) and *n*-butanol (10 mL). The mixture was refluxed with a Dean–Stark apparatus for 20 h. The solvent was evaporated in vacuo to afford the crude product, which was purified by silica gel column chromatography using EtOAC/methanol (20:1) as an eluent to give a blue solid (yield: 0.768 g, 62%). Mp 234 °C; ^{1}H NMR (300 MHz, $CDCl_3$): δ (ppm) 8.27–8.24 (d, J=8.7 Hz, 1H), 8.16 (s, 1H), 7.44–7.30 (m, 3H), 7.17–7.14 (d, J=7.9 Hz, 1H), 6.95–6.92 (d, J=8.8 Hz, 1H), 6.10 (s, 1H), 5.97 (s, 1H), 3.73 (s, 3H), 3.51 (s, 3H), 1.83 (s, 6H), 1.80 (s, 6H); ^{13}C NMR (75 MHz, $CDCl_3$): δ (ppm) 185.6, 176.6, 174.6, 166.7, 148.5, 142.9, 142.4, 142.3, 142.2, 128.1, 125.4, 125.3, 122.4, 118.1, 110.4, 107.5, 89.1, 88.2, 50.3, 47.8, 31.6, 30.5, 27.3, 26.5; ATR-FTIR (KBr, cm^{-1}): 3023, 2965, 2924, 1602, 1500, 1476, 1261, 1214, 797, 744, 733; MALDI-TOF MS, m/z: calcd for $C_{28}H_{27}N_3O_4$: 469.200, found: 469.543 $[M]^+$.

*4.2.13. (Z)-4-((5-Amino-1,3,3-trimethyl-3H-indolium-2-yl)methylene)-3-oxo-2-((Z)-(1,3,3-trimethylindolin-2-ylidene)methyl)cyclobut-1-enolate (**16**).* A mixture of **15** (0.5 g, 1.06 mmol) and tin(II) chloride dihydrate (1.674 g, 7.42 mmol) was refluxed in a mixture of ethanol (15 mL) and concentrated HCl (2 mL) for 8 h. After cooling to room temperature, the mixture was poured into cold water and neutralized with 2 N NaOH. The mixture was extracted with CH_2Cl_2, and the organic layer was dried over Na_2SO_4. The solvent was evaporated to afford a crude solid, which was purified by silica gel column chromatography using EtOAC/methanol (20:1) as an eluent to give a blue solid (yield: 0.406 g, 87%). Mp 240 °C; ^{1}H NMR (300 MHz, $CDCl_3$): δ (ppm) 7.33–7.28 (m, 2H), 7.12–7.07 (t, J=7.4 Hz, 1H), 6.95–6.93 (d, J=7.7 Hz, 1H), 6.85–6.82 (d, J=8.3 Hz, 1H), 6.72 (s, 1H), 6.65–6.62 (d, J=7.6 Hz, 1H), 5.86 (s, 2H), 3.84 (s, 2H), 3.57 (s, 3H), 3.47 (s, 3H), 1.78 (s, 6H), 1.74 (s, 6H); ^{13}C NMR (75 MHz, $CDCl_3$): δ (ppm) 179.6, 176.2, 170.9, 168.8, 144.2, 143.7, 143.1, 141.8, 135.0, 127.6, 123.0, 122.1, 113.9, 110.4, 109.8, 108.5, 86.3, 49.6, 48.6, 31.2, 30.2, 29.7, 27.1, 26.8; ATR-FTIR (KBr, cm^{-1}): 3319, 3224, 2960, 2923, 2854, 1736, 1569, 1480, 1418, 1373, 1263, 1217, 1089, 1054, 1040, 932, 963, 789, 729; MALDI-TOF MS, m/z: calcd for $C_{28}H_{29}N_3O_2$: 439.226, found: 440.008 $[M]^+$.

*4.2.14. 3-(5′-(1-(4-Butylphenyl)-1H-phenanthro[9,1 0-d]imidazol-2-yl)-2, 2′-bithiophen-5-yl)-2-cyanoacrylic acid (**H6**).* Piperidine (0.092 mL, 0.93 mmol) was added to a mixture of **3** (0.17 g, 0.31 mmol) and cyanoacetic acid (0.053 g, 0.62 mmol) dissolved in acetonitrile (20 mL) and THF (10 mL). The mixture was refluxed overnight and then allowed to cool to room temperature. Water was added, and the mixture was extracted with CH_2Cl_2, and dried over Na_2SO_4. The solvent was evaporated in vacuo to afford the crude product, which was purified by silica gel column chromatography using CH_2Cl_2/methanol (5:1) and recrystallized with CH_2Cl_2 and hexane to give a reddish-brown solid (yield: 0.13 g, 69%). Mp 234 °C; ^{1}H NMR (300 MHz, DMSO-d_6): δ (ppm) 8.93–8.90 (d, J=8.4 Hz, 1H), 8.88–8.85 (d, J=8.5 Hz, 1H), 8.66–8.64 (d, J=8 Hz, 1H), 8.03 (s, 1H), 7.80–7.62 (m, 8H), 7.58–7.53 (t, J=7.5 Hz, 1H), 7.45–7.44 (d, J=3.9 Hz, 1H), 7.34–7.30 (m, 2H), 7.13–7.10 (d, J=8 Hz, 1H), 6.63–6.61 (d, J=4 Hz, 1H), 2.88–2.84 (t, J=7.4 Hz, 2H), 1.77–1.72 (t, J=7.4 Hz, 2H), 1.45–1.38 (q, J=7.4 Hz, 2H), 1.00–0.96 (t, J=7.3 Hz, 3H); ^{13}C NMR (125 MHz, DMSO-d_6): δ (ppm) 162.9, 145.6, 144.7, 144.6141.0, 137.0, 136.8, 136.7, 135.0, 132.7, 130.7, 128.7, 128.6, 128.0, 127.8, 127.5, 126.7, 126.2, 125.9, 125.8, 125.6, 125.0, 124.8, 124.5, 123.7, 122.1, 122.0, 120.0, 119.2, 118.0, 110.3, 34.5, 32.9, 21.5, 13.8; ATR-FTIR (KBr, cm^{-1}): 3460, 3035, 2955, 2930, 2861, 2206, 1627, 1578, 1517, 1435, 1302, 1233, 1136,939, 785, 748, 720; HRMS, m/z: calcd for $C_{37}H_{27}N_3O_2S_2$: 609.1545, found 610.1617 $[M+H]^+$.

*4.2.15. (E)-3-(5′-(4-(1-(4-Butylphenyl)-1H-phenanthro[9,10-d]imidazol-2-yl)phenyl)-2,2′-bithiophen-5-yl)-2-cyanoacrylic acid (**H7**).* **H7** was prepared according to the synthetic procedure for **H6**, using **8** instead of **3**. The crude product was purified by silica gel column chromatography using CH_2Cl_2/methanol (10:1) as an eluent to give an orange solid (yield: 71%). Mp 246 °C; ^{1}H NMR (300 MHz, DMSO-d_6): δ (ppm) 9.07 (s, 2H), 8.93–8.90 (d, J=8.5 Hz, 1H), 8.88–8.85 (d, J=8.4 Hz, 1H), 8.71–8.69 (d, J=7.7 Hz, 1H), 8.13 (s, 1H), 7.79–7.74 (t, J=7.2 Hz, 1H), 7.71–7.57 (m, 8H), 7.54–7.48 (m, 5H), 7.32–7.27 (t, J=7.9 Hz, 1H), 7.10–7.07 (d, J=8.2 Hz, 1H), 2.81–2.76 (t, J=7.3 Hz, 2H), 1.57–1.54 (t, J=5.6 Hz, 2H), 1.40–1.33 (q, J=7.4 Hz, 2H), 0.98–0.93 (t, J=7.2 Hz, 3H); ^{13}C NMR (125 MHz, DMSO-d_6): δ (ppm) 163.6, 149.7, 144.7, 142.8, 141.1, 140.4, 136.6, 136.5, 135.9, 135.7, 135.4, 133.2, 130.2, 129.6, 129.5, 128.8, 128.5, 128.0, 127.7, 127.4, 127.0, 126.6, 126.5, 125.9, 125.8, 125.2, 124.9, 124.7, 124.5, 123.5, 122.4, 122.0, 120.2, 119.0, 108.9, 34.4, 32.8, 22.1, 13.8; ATR-FTIR (KBr, cm^{-1}): 3566, 3057, 2953, 2929, 2859, 2213, 1602, 1515, 1435, 1379, 1226, 1158, 1096, 1049, 943, 842, 796, 742, 723; HRMS, m/z: calcd for $C_{43}H_{31}N_3O_2S_2$: 685.1858, found 686.1945 $[M+H]^+$.

*4.2.16. (E)-3-(5′-(4′-(1-(4-butylphenyl)-1H-phenanthro[9,10-d]imidazol-2-yl)biphenyl-4-yl)-2,2′-bithiophen-5-yl)-2-cyanoacrylic acid (**H8**).* **H8** was prepared according to the synthetic procedure for **H6**, using **9** instead of **3**. The crude product was purified by silica gel column chromatography using CH_2Cl_2/methanol (10:1) as an eluent to give a yellow solid (yield: 60%). Mp 258 °C; ^{1}H NMR (300 MHz, DMSO-d_6): δ (ppm) 8.95–8.92 (d, J=8.6 Hz, 1H), 8.90–8.87 (d, J=8.5 Hz, 1H), 8.72–8.70 (d, J=7.8 Hz, 1H), 8.42 (s, 2H), 8.05 (s, 1H), 7.80–7.63 (m, 10H), 7.59–7.51 (m, 8H), 7.35–7.30 (t, J=8.0 Hz, 1H), 7.12–7.09 (d, J=8.2 Hz, 1H), 2.82–2.77 (t, J=7.3 Hz, 2H), 1.57–1.54 (t, J=4.5 Hz, 2H), 1.41–1.33 (q, J=7.2 Hz, 2H), 0.98–0.93 (t, J=7.2 Hz, 3H); ^{13}C NMR (125 MHz, DMSO-d_6): δ (ppm) 163.3, 150.0, 144.7, 143.6, 141.0, 139.3, 138.4, 136.5, 135.8, 135.0, 133.5, 132.4, 130.2, 129.5, 128.8, 128.5, 128.0, 127.7, 127.4, 127.3, 127.0, 126.7, 126.5, 126.2, 126.1, 125.9, 125.7, 125.5, 125.4, 125.2, 124.6, 124.5, 123.6, 122.5, 122.4, 122.0, 120.2, 110.1, 34.4, 32.8, 22.2, 13.8; ATR-FTIR (KBr, cm^{-1}): 3566, 2948, 2928, 2854, 2211, 1608, 1592, 1514, 1465, 1452, 1380, 1235, 1145, 1032, 947, 830, 795, 753, 729; HRMS, m/z: calcd for $C_{49}H_{35}N_3O_2S_2$: 761.2171, found 762.2251 $[M+H]^+$.

*4.2.17. (E)-2-Cyano-3-(5′-(4-(1-(4-(2-(2-(2-methoxyethoxy)ethoxy) ethoxy)phenyl)-1H-phenanthro[9,1 0-d]imidazol-2-yl)phenyl)-2,2′-bithiophen-5-yl)ac-rylic acid (**H9**).* **H9** was prepared according to the synthetic procedure for **H6**, using **13** instead of **3**. The crude product was purified by silica gel column chromatography using

CH_2Cl_2/methanol (10:1) as an eluent to give a red solid (yield: 0.145 g, 65%). Mp 214 °C; ^{1}H NMR (500 MHz, DMSO-d_6): δ (ppm) 8.91–8.90 (d, J=8.5 Hz, 1H), 8.86–8.85 (d, J=8.7 Hz, 1H), 8.70–8.68 (d, J=8 Hz, 1H), 8.05 (s, 1H), 7.77–7.74 (t, J=7.1 Hz, 1H), 7.72–7.68 (m, 2H), 7.67–7.62 (m, 8H), 7.56–7.53 (t, J=7.1 Hz, 1H), 7.50–7.49 (d, J=3.8 Hz, 1H), 7.47–7.46 (d, J=3.8 Hz, 1H), 7.40–7.36 (t, J=7.3 Hz, 1H), 7.24–7.23 (d, J=8.9 Hz, 2H), 7.19–7.18 (d, J=8.4 Hz, 1H), 4.23–4.22 (t, J=3 Hz, 2H), 3.83–3.81 (t, J=4.4 Hz, 2H), 3.64–3.62 (m, 2H), 3.57–3.55 (m, 2H), 3.54–3.52 (m, 2H), 3.44–3.42 (m, 2H), 3.22 (s, 3H); ^{13}C NMR (125 MHz, DMSO-d_6): δ (ppm) 163.3, 159.4, 149.9, 142.8, 140.8, 140.1, 136.5, 136.2, 136.0, 135.4, 133.1, 130.6, 130.2, 129.6, 129.5, 128.5, 128.1, 127.7, 127.4, 126.9, 126.7, 125.9, 125.7, 125.2, 124.9, 124.6, 124.4, 123.6, 122.5, 122.0, 120.2, 119.2, 115.9, 109.6, 71.3, 70.0, 69.8, 69.6, 68.9, 67.6, 64.8, 58.0; ATR-FTIR (KBr, cm^{-1}): 3566, 3036, 2939, 2925, 2870, 2210, 1738, 1606, 1511, 1450, 1373, 1296, 1248, 1108, 941, 840, 794, 755, 723; HRMS, m/z: calcd for $C_{46}H_{37}N_3O_6S_2$: 791.2124, found: 792.2207 $[M+H]^+$.

*4.2.18. (Z)-4-((5-(2-(4-(5′-((Z)-2-Carboxy-2-cyano-vinyl)-2,2′-bithiophen-5-yl)phenyl)-1H-phenanthro-[9,10-d]imidazol-1-yl)-1,3,3-trimethyl-3H-indoliu-m-2-yl)methylene)-3-oxo-2-((Z)-(1,3,3-trimethylindolin-2-ylidene)methyl)cyclobut-1-enolate (**H10**).* **H10** was prepared according to the synthetic procedure for **H6**, using **18** instead of **3**. The crude product was purified by silica gel column chromatography using CH_2Cl_2/methanol (10:1) as an eluent to give a green solid (yield: 0.080 g, 68%). Mp 317 °C; ^{1}H NMR (300 MHz, DMSO-d_6): δ (ppm) 8.95–8.88 (m, 2H), 8.73–8.71 (d, J=7.6 Hz, 1H), 8.00 (s, 2H), 7.89 (s, 1H), 7.79–7.65 (m, 8H), 7.56–7.47 (m, 5H), 7.39–7.37 (m, 3H), 7.24–7.21 (d, J=7.5 Hz, 2H), 5.84 (s, 1H), 5.80 (s, 1H), 5.51 (s, 1H), 3.65 (s, 3H), 3.63 (s, 3H), 1.74 (s, 6H), 1.70 (s, 6H); ^{13}C NMR (125 MHz, DMSO-d_6): δ (ppm) 181.4, 181.1, 180.7, 180.3, 177.3, 175.1, 173.7, 171.4, 168.1, 165.1, 162.9, 149.9, 144.4, 144.0, 142.7, 142.6, 141.6, 140.7, 139.8, 136.6, 136.5, 136.1, 135.4, 133.2, 132.7, 132.2, 131.5, 129.5, 129.4, 128.5, 128.1, 127.9, 127.7, 127.4, 126.9, 126.6, 125.9, 125.8, 125.3, 125.0, 124.6, 124.5, 124.3, 123.7, 123.4, 122.5, 122.2, 122.0, 120.3, 119.2, 110.8, 87.0, 84.4, 49.0, 48.2, 27.0, 26.5, 26.2, 25.9; ATR-FTIR (KBr, cm^{-1}): 3565, 2924, 2852, 2211, 1732, 1601, 1543, 1481, 1458, 1364, 1270, 1225, 1097, 1068, 923, 838, 791, 754, 723; HRMS, m/z: calcd for $C_{61}H_{45}N_5O_4S_2$: 975.2913, found: 976.2972 $[M+H]^+$.

4.3. Device fabrication

Dye-sensitized solar cell device fabrication: Fluorine-doped tin oxide (FTO) glass plates (Pilkington, 8 Ω sq^{-1}, 2.3 mm thick) were cleaned in a detergent solution in an ultrasonic bath for 15 min then rinsed with water and ethanol. The washed FTO glass plates were immersed in a 40 mM $TiCl_4$ aqueous solution at 70 °C for 30 min. A transparent nanocrystalline layer was deposited on the FTO glass by the doctor blade printing method using TiO_2 paste (Solaronix, Ti-Nanoxide T/SP) and a scattering layer paste (CCIC, PST-400C). The TiO_2 layer was gradually sintered according to a programmed procedure. The sintered layers consisted of a transparent layer (7 μm thick) and a scattering layer (4 μm thick). The TiO_2 electrodes were again treated with $TiCl_4$ at 70 °C for 30 min and sintered at 500 °C for 30 min. Subsequently, the TiO_2 electrodes were immersed in solutions of the dyes in 0.3 mM DMF : EtOH (1:2) containing 10 mM Chenodeoxycholic acid (CDCA) at room temperature for 18 h in the dark. The FTO plates for the counterelectrodes were cleaned in an ultrasonic bath containing H_2O, acetone and 0.1 M HCl. Next, counterelectrodes were prepared by coating each FTO plate with a drop of H_2PtCl_6 solution (2 mg of Pt in 1 mL of ethanol) and heating them to 400 °C for 15 min, causing the dye adsorbed on the TiO_2 electrode to adhere to the counterelectrode by coverage with a hot-melt polymer film (Surlyn 1702, 100 mm thick, DuPont). A drop of electrolyte solution (0.6 M 1,2-dimethyl-3-n-propylimidazolium iodide (DMPImI), 0.05 M iodine, ~~0~~–0.5 M *tert*-butylpyridine, and 0.1 M LiI in acetonitrile) was injected though a hole in the counterelectrode and driven into the cell by vacuum backfilling. Finally, the hole was sealed using a hot-melt polymer film and a cover glass (0.1 mm thick).

Acknowledgements

This work was supported by a grant for the Center for Next-Generation Dye-Sensitized Solar Cells (No. 2012-0000591) from the Basic Science Research Program through the National Research Foundation of Korea (NRF) funded by the Ministry of Education, Science and Technology (MEST) of Korea.

Supplementary data

Supplementary data related to this article can be found online at doi:10.1016/j.tet.2012.04.074.

References and notes

1. O'Regan, B.; Grätzel, M. *Nature* **1991**, *353*, 737.
2. (a) Nazeeruddin, M. K.; Kay, A.; Rodicio, L.; Humphry-Baker, R.; Müller, E.; Liska, P.; Vlachopoulos, N.; Grätzel, M. *J. Am. Chem. Soc.* **1993**, *115*, 6382; (b) Nazeeruddin, M. K.; Zakeeruddin, S. M.; Humphry-Baker, R.; Jirousek, M.; Liska, P.; Vlachopoulos, N.; Grätzel, M. *Inorg. Chem.* **1999**, *38*, 6298; (c) Nazeeruddin, M. K.; Pechy, P.; Renouard, T.; Zakeeruddin, S. M.; Humphry-Baker, R.; Comte, P.; Liska, P.; Cevey, L.; Costa, E.; Shklover, V.; Spiccia, L.; Deacon, G. B.; Bignozzi, C. A.; Grtäzel, M. *J. Am. Chem. Soc.* **2001**, *123*, 1613; (d) Gao, F.; Wang, Y.; Shi, D.; Zhang, J.; Wang, M.; Jing, X.; Humphry-Baker, R.; Wang, P.; Zakeeruddin, S. M.; Grätzel, M. *J. Am. Chem. Soc.* **2008**, *130*, 10720.
3. Fischer, M. K. R.; Wenger, S.; Wang, M.; Mishra, A.; Zakeerud-din, S. M.; Grätzel, M.; Bäuerle, P. *Chem. Mater.* **2010**, *22*, 1836.
4. Zeng, W.; Cao, Y.; Bai, Y.; Wang, Y.; Shi, Y.; Zhang, M.; Wang, F.; Pan, C.; Wang, P. *Chem. Mater.* **2010**, *22*, 1915.
5. Mishra, A.; Fischer, M. K.; Bäuerle, P. *Angew. Chem., Int. Ed.* **2008**, *48*, 2474.
6. (a) Hagberg, D. P.; Marinado, T.; Karlsson, K. M.; Nonomura, K.; Qin, P.; Boschloo, G.; Brinck, T.; Hagfeldt, A.; Sun, L. *J. Org. Chem.* **2007**, *72*, 9550; (b) Li, G.; Jiang, K. J.; Li, Y. F.; Li, S. L.; Yang, L. M. *J. Phys. Chem. C* **2008**, *112*, 13591; (c) Xu, M.; Wenger, S.; Bala, H.; Shi, D.; Li, R.; Zhou, Y.; Zakeeruddin, S. M.; Grätzel, M.; Wang, P. *J. Phys. Chem. C* **2009**, *113*, 2966; (d) Tian, H.; Yang, X.; Chen, R.; Zhang, R.; Hagfeldt, A.; Sun, L. *J. Phys. Chem. C* **2008**, *112*, 11023.
7. (a) Choi, H.; Baik, C.; Kang, S. O.; Ko, J.; Kang, M.-S.; Nazeeruddin, M. K.; Grätzel, M. *Angew. Chem., Int. Ed.* **2008**, *47*, 327; (b) Hwang, S.; Lee, J. H.; Park, C.; Lee, H.; Kim, C.; Park, C.; Lee, M.-H.; Lee, W.; Park, J.; Kim, K.; Park, N.-G.; Kim, C. *Chem. Commun.* **2007**, *43*, 4887; (c) Wang, Z. S.; Koumura, N.; Cui, Y.; Takahashi, M.; Sekiguchi, H.; Mori, A.; Kubo, T.; Furube, A.; Hara, K. *Chem. Mater.* **2008**, *20*, 3993; (d) Ning, Z. J.; Zhang, Q.; Wu, W. J.; Pei, H. C.; Liu, B.; Tian, H. *J. Org. Chem.* **2008**, *73*, 3791.
8. (a) Tsai, M. S.; Hsu, Y. C.; Lin, J. T.; Chen, H. C.; Hsu, C. P. *J. Phys. Chem. C* **2007**, *111*, 18785; (b) Kumar, D.; Thomas, K. R. J.; Lee, C. P.; Ho, K. C. *Org. Lett.* **2011**, *13*, 2622; (c) Velusamy, M.; Hsu, Y.-C.; Lin, J. T.; Chang, C.-W.; Hsu, C.-P. *Chem.—Asian. J.* **2010**, *5*, 87.
9. (a) Chen, R.; Yang, X.; Tian, H.; Wang, X.; Hagfeldt, A.; Sun, L. *Chem. Mater.* **2007**, *19*, 4007; (b) Chang, Y. J.; Chow, T. J. *Tetrahedron* **2009**, *65*, 4726.
10. (a) Snaith, H. J.; Zakeeruddin, S. M.; Schmidt-Mende, L.; Klein, C.; Grätzel, M. *Angew. Chem., Int. Ed.* **2005**, *44*, 6413; (b) Snaith, H. J.; Moule, A. J.; Klein, C.; Meerholz, K.; Friend, R. H.; Grätzel, M. *Nano. Lett.* **2007**, *7*, 3372.
11. (a) Choi, H.; Kim, J. J.; Song, k.; Ko, J.; Nazeeruddin, M. K.; Grätzel, M. *J. Mater. Chem.* **2010**, *20*, 3280; (b) Paek, S.; Choi, H.; Kim, C.; Cho, N.; So, S.; Song, K.; Nazeeruddin, M. K.; Ko, J. *Chem. Commun.* **2011**, *47*, 2874.
12. (a) Bahr, J. L.; Yang, J.; Kosynkin, D. V.; Bronikowski, M. J.; Smalley, R. E.; Tour, J. M. *J. Am. Chem. Soc.* **2001**, *123*, 6536; (b) Keil, D.; Hartmann, H. *Dyes Pig.* **2001**, *49*, 161; (c) Lee, W.; Cho, N.; Kwon, J.; Ko, J.; Hong, J.-I. *Chem.—Asian. J.* **2012**, *7*, 343.
13. Chang, Y. J.; Chow, T. J. *Tetrahedron* **2009**, *65*, 9626.
14. McEwen, J. J.; Wallace, K. J. *Chem. Commun.* **2009**, *45*, 6339.
15. (a) Yum, J. H.; Walter, P.; Huber, S.; Rentsch, D.; Geiger, T.; Nüesch, F.; Angelis, F. D.; Grätzel, M.; Nazeeruddin, M. K. *J. Am. Chem. Soc.* **2007**, *129*, 10320; (b) Geiger, T.; Kuster, S.; Yum, J. H.; Moon, S. J.; Nazeeruddin, M. K.; Grätzel, M.; Nüesch, F. *Adv. Funct. Mater.* **2009**, *19*, 2720; (c) Li, J. Y.; Chen, C. Y.; Lee, C. P.; Chen, S. C.; Lin, T. H.; Tsai, H. H.; Ho, K. C.; Wu, C. G. *Org. Lett.* **2010**, *12*, 5454.
16. (a) Teng, C.; Yang, X.; Yang, C.; Li, S.; Cheng, M.; Hagfeldt, A.; Sun, L. *J. Phys. Chem. C* **2010**, *114*, 9101; (b) Wang, Z. S.; Hara, K.; Dan-oh, Y.; Kasada, C.; Shinpo, A.; Suga, S.; Arakawa, H.; Sugihara, H. *J. Phys. Chem. C* **2005**, *109*, 3907.
17. Hagfeldt, A.; Grätzel, M. *Chem. Rev.* **1995**, *95*, 49.
18. Nakade, S.; Kanzaki, T.; Kubo, W.; Kitamura, T.; Wada, Y.; Yanagid, S. *J. Phys. Chem. B* **2005**, *109*, 3480.
19. Wu w.; Yang J.; Hua J.; Tang J.; Zhang L.; Long Y.; Tian H. J. Mater. Chem. 2010, , 1772.
20. (a) Wang, E.; Meng, Q.; Wang, C.; Li, L.; Li, H.; Hu, W. *Synth. Met.* **2009**, *159*, 1298; (b) Berezin, M. Y.; Guo, K.; Teng, B.; Edwards, W. B.; Anderson, C. J.; Vasalatiy, O.; Gandjbakhche, A.; Griffiths, G. L.; Achilefu, S. *J. Am. Chem. Soc.* **2009**, *131*, 9198.